Stability of a quantum skyrmion: Projective measurements and the quantum Zeno effect

Fabio Salvati,* Mikhail I. Katsnelson, Andrey A. Bagrov, and Tom Westerhout
Institute for Molecules and Materials, Radboud University, Heijendaalseweg 135, 6525 AJ Nijmegen, Netherlands

(Received 23 August 2023; revised 21 December 2023; accepted 19 January 2024; published 9 February 2024)

Magnetic skyrmions are vortexlike quasiparticles characterized by long lifetime and remarkable topological properties. That makes them a promising candidate for the role of information carriers in magnetic information storage and processing devices. Although considerable progress has been made in studying skyrmions in classical systems, little is known about the quantum case: quantum skyrmions cannot be directly observed by probing the local magnetization of the system, and the notion of topological protection is elusive in the quantum realm. Here we explore the potential robustness of quantum skyrmions in comparison to their classical counterparts. We theoretically analyze the dynamics of a quantum skyrmion subject to local projective measurements and demonstrate that the properties of the skyrmionic quantum state change very little upon external perturbations. We further show that by performing repetitive measurements on a quantum skyrmion, it can be completely stabilized through an analog of the quantum Zeno effect.

DOI: 10.1103/PhysRevB.109.064409

I. INTRODUCTION

Magnetic skyrmions are nanometer-size topological spin textures with integer topological charges and long lifetimes [1–6]. Topological Hall effect and current-driven motion of skyrmions with low-power consumption can be exploited for future applications of memory devices as well as information carriers [7,8]. The general contemporary tendency to ultraminiaturization of such elements results naturally in attempts to study the regime when quantum effects become decisive, and that brings us to the topic of quantum skyrmions [9–17]. Contrary to classical skyrmions, quantum skyrmions are not topologically protected in a rigorous sense by the existence of a conserving topological charge. Nonetheless, a quantum analog of the topological invariant has been proposed [10,17]. By studying the scalar chirality, defined as a local three-spin correlation function, it is indeed possible to characterize a quantum skyrmion, but the scalar chirality is, formally, not a topological charge [18]. The relation between a quantum skyrmion state and its classical counterpart turns out to be highly nontrivial [17], and the robustness of the quantum skyrmion phase is not guaranteed. However, for any potential applications, the robustness property is crucial and its analysis in the quantum case deserves special attention.

In this paper, we study the effect of a few consecutive projective measurements on the stability of a quantum skyrmion state on the 19-site triangular lattice [10,16,17]. We demonstrate the robustness of the quantum skyrmion in terms of chirality as well as the spin-spin correlation function, which is, in principle, easier accessible experimentally. This is an encouraging result since a projective measurement [19] is an idealization of the real physical process of reading information from a quantum device.

Another aim of our paper is to use quantum skyrmions as a model system to study the general issues of the theory of quantum measurements. Here we focus on one concept from this theory, namely, the quantum Zero effect [20–22], which is a counterintuitive effect of repeating projective measurements stabilizing an excited state of the quantum system. Discreteness of the energy spectrum of the system is very important for the quantum Zeno effect (QZE), and its applicability for a 19-site quantum skyrmion, that is large enough to consider its spectrum quasicontinuous, is not clear. We show that, nevertheless, an analog of the QZE exists in this situation, and discuss possible reasons.

II. DYNAMICS OF A QUANTUM SKYRMION

A. Model

In this paper, we consider the quantum spin Heisenberg model with Dzyaloshinskii-Moriya interaction (DMI) and external magnetic field. Its Hamiltonian reads

$$H = \sum_{\langle i,j\rangle} J_{ij}\, \boldsymbol{S}_i \cdot \boldsymbol{S}_j + \sum_{\langle i,j\rangle} \mathbf{D}_{ij} \cdot [\boldsymbol{S}_i \times \boldsymbol{S}_j] + \sum_i B\, S_i^z, \qquad (1)$$

where $\boldsymbol{S}_i = \frac{1}{2}(\sigma_i^x,\ \sigma_i^y,\ \sigma_i^z)$, σ_i^α for $\alpha \in \{x, y, z\}$, are the Pauli matrices on the ith site, and $\langle i, j\rangle$ denote the pairs of the nearest neighbors. $\mathbf{D}_{ij}$ is an in-plane vector perpendicular to the bond (i, j). We will focus on the case of zero temperature, that is, we will work with the ground state of the Hamiltonian. We will characterize the quantum skyrmion by the quantum scalar chirality (further called just chirality for brevity),

$$Q = \langle \hat{Q} \rangle = \frac{1}{\pi} \sum_{\langle ijk\rangle} \langle \boldsymbol{S}_i \cdot [\boldsymbol{S}_j \times \boldsymbol{S}_k] \rangle, \qquad (2)$$

where the sum runs over all nonoverlapping triangular plaquettes. The quantity Q is a local three-spin correlation function defined on the neighboring lattice sites, and was introduced

*fabio.salvati@ru.nl

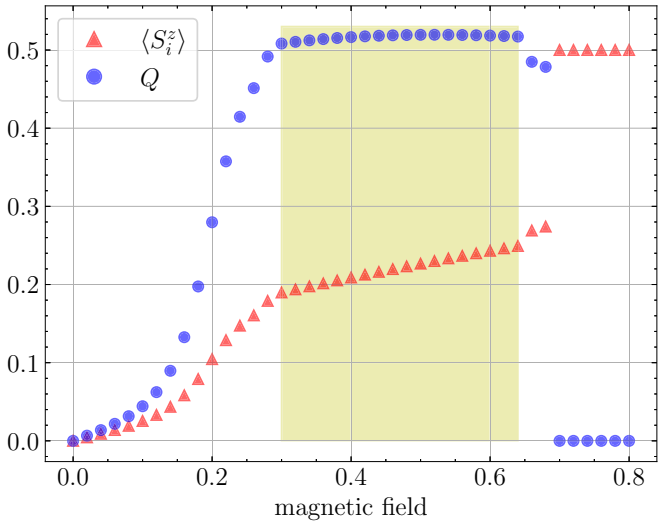

FIG. 1. Ground-state phase diagram of the Hamiltonian Eq. (1) on the 19-site triangular lattice with periodic boundary conditions. The chirality Q is shown in blue circles and the magnetization $\langle S_i^z \rangle$ is shown in red triangles, both as functions of the external magnetic field B. In the ground state, $\langle S_i^z \rangle$ is the same for every site i. The quantum skyrmion phase is highlighted in yellow.

[10,23] as the quantum analog of the skyrmion topological index:

$$Q_{\text{top}} = \frac{1}{4\pi} \int \mathbf{m} \cdot [\partial_x \mathbf{m} \times \partial_y \mathbf{m}] \mathrm{d}x\, \mathrm{d}y.$$

However, Q is not a topological invariant in a mathematically rigorous sense. Physically speaking, it is subjected to quantum spin fluctuations. Nevertheless, it does characterize the quantum skyrmion phase since, in the corresponding state, it displays unambiguously a nonzero and nearly constant value as a function of the external parameters, see Fig. 1.

Exact diagonalization code [24] has been applied to numerically solve the Hamiltonian Eq. (1) for a 19-site triangular lattice with periodic boundary conditions. Following the previous works [10,16], we set $J_{ij} = J = -0.5D$, where $D = 1$ is the length of the DMI vectors $\mathbf{D}_{ij}$. Figure 1 is in excellent agreement with previous studies, but we nevertheless show it here as a basis for further calculations.

In Fig. 1, we show the dependence of the chirality on the external magnetic field. For $0.30 \leqslant B \leqslant 0.64$, Q is nonzero and nearly constant, and we associate this region with the quantum skyrmion phase. Below $B = 0.30$, the system will slowly approach the helical spin state configuration at $B = 0$, where both chirality and magnetization go to zero. Above $B = 0.64$, a first-order transition happens and the system becomes a saturated ferromagnet. Full characterization of these phases can be found in Ref. [10], and in this paper we use these results as a starting point for studying the robustness of a quantum skyrmion state.

B. Quench dynamics following a projective measurement

In any practical sense, robustness of a physical system should be understood as (partial) stability of its relevant properties under external deformations and environmental

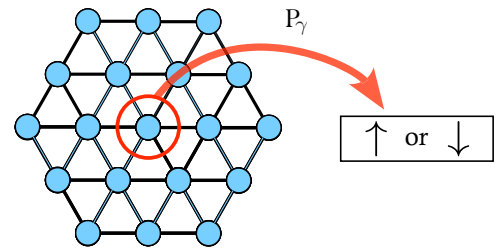

FIG. 2. Illustration of the projective measurement. The projection operator P_γ (where γ is either $\uparrow$ or $\downarrow$) acts on the center site of the lattice, and the center spin becomes either $|\uparrow\rangle$ or $|\downarrow\rangle$ after the projection.

effects. For a quantum skyrmion, although there is no notion of topological protection, if it is possible to show that its characteristic features do not change significantly upon strong perturbations, one can claim that the quantum skyrmion indeed shares the property of stability with its classical counterpart. In light of great hope that skyrmions can provide a physical ground for dense information storage, it is natural to analyze their stability upon the act of reading information. The latter, in its minimal form, can be modeled as a projective measurement of components of one or a few spins [25–27]. The single site measurement protocol is shown in Fig. 2. Two natural cases to be considered are the measurement of the z and x components of a single spin (i.e., the σ^z and σ^x operators). The former can be regarded as the most classical measurement, since it is aligned with the external magnetic field and has a clear classical counterpart, and the latter, which is transversal to the magnetic field, can be viewed as the most quantum one.

Formally, the single-site projective measurement [19,28–32] can be described with the following operator acting on the quantum skyrmion ground-state wave function $|\psi_{\text{GS}}\rangle$:

$$P_\gamma^k = \mathbb{1}_2 \otimes \cdots \otimes |\gamma\rangle\langle\gamma|_k \otimes \cdots \otimes \mathbb{1}_2,$$

where k is the index of the measured site, γ is either $\uparrow$ or $\downarrow$ along the x or z axis, and $\mathbb{1}_2$ is the 2×2 identity matrix. Immediately after the projective measurement, the kth spin of the cluster will be oriented along the chosen axis as shown in Fig. 2. In what follows, we will always consider the measurement of the central site and will omit the index k in the expressions.

Since $|\psi_{\text{GS}}\rangle$ is a pure state, its density matrix is simply $\rho = |\psi_{\text{GS}}\rangle\langle\psi_{\text{GS}}|$. Then, by denoting the state right after the measurement as

$$|\psi_\gamma\rangle \equiv \frac{P_\gamma |\psi_{\text{GS}}\rangle}{\sqrt{\langle\psi_{\text{GS}}|P_\gamma|\psi_{\text{GS}}\rangle}},$$

and according to the von Neumann theory of measurements [19], the two possible outcomes of the measurement can be combined into the new density matrix:

$$\rho = \sum_{\gamma\in\{\uparrow,\downarrow\}} p_\gamma |\psi_\gamma\rangle\langle\psi_\gamma|, \quad \text{where} \sum_{\gamma\in\{\uparrow,\downarrow\}} p_\gamma = 1, \tag{3}$$

and the probabilities p_γ are given by

$$p_\gamma = \langle\psi_{\text{GS}}|P_\gamma|\psi_{\text{GS}}\rangle. \tag{4}$$

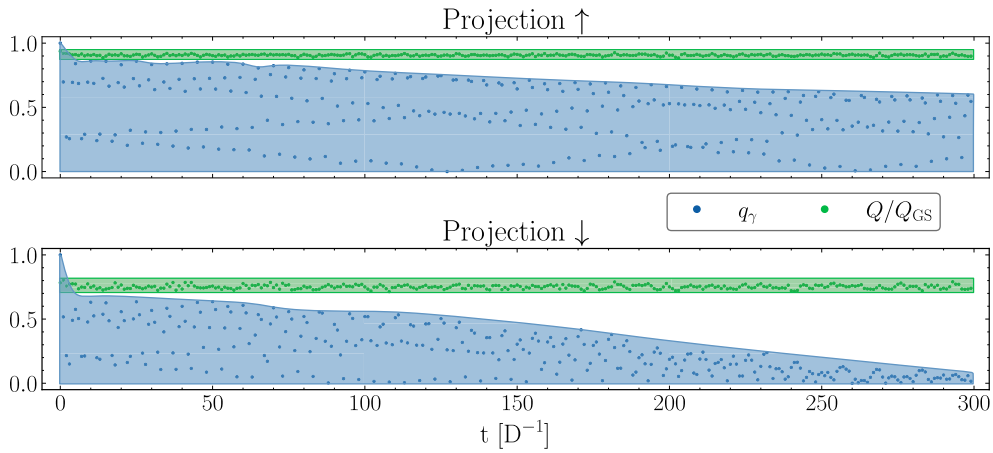

FIG. 3. Time evolution of the chirality Q (dark green dots) and overlap q_γ (blue dots) after one σ^z projective measurement. The top panel shows the projection onto $|\uparrow_z\rangle$ and the bottom panel—onto $|\downarrow_z\rangle$. Lines and shades are a guide to eye.

The state $|\psi_\gamma(0)\rangle = |\psi_\gamma\rangle$ then undergoes a unitary evolution with the Hamiltonian Eq. (1),

$$|\psi_\gamma(t)\rangle = e^{-itH}|\psi_\gamma(0)\rangle = U(t)|\psi_\gamma(0)\rangle, \tag{5}$$

where we have introduced the time evolution operator $U(t) = \exp(-itH)$. To compute the quantum state evolution, we expand $U(t)$ in terms of the Chebyshev polynomials [33,34],

$$U(t) = \exp(-i\tau\mathcal{G}) = \sum_{k=0}^{\infty} \alpha_k(-i)^k J_k(\tau)T_k(\mathcal{G}), \tag{6}$$

where T_k are the Chebyshev polynomials of order k, $J_k(\tau)$ are the Bessel functions, $\tau = E_{\max}t/2 \to \tau = (E_{\max} - E_{\min})t/2$, $\alpha_k = 1$ for $k = 0$ and $\alpha_k = 2$ for $k \geqslant 1$, and $\mathcal{G}$ is a rescaled Hamiltonian defined as

$$\mathcal{G} = \frac{2H - (E_{\max} + E_{\min})}{2(E_{\max} - E_{\min})},$$

with $E_{\min}$ and $E_{\max}$ being the minimal and maximal eigenvalues of H, respectively. The spectrum of $\mathcal{G}$ then lies in the range $[-1, 1]$, which ensures the convergence of the series Eq. (6).

High accuracy of this method is guaranteed by the super-exponential decay of the Bessel functions, and truncating the series at 40 Chebyshev polyniomals lead to numerically exact results for the time intervals considered in this paper.

III. ROBUSTNESS

Let us now discuss the results of numerical simulations. We fix the magnetic field $B = 0.5$ such that the ground state lies deep in the skyrmionic phase. A projective measurement is then performed on the center site at time $t = 0$, and the two possible outcomes are $|\psi_\uparrow(0)\rangle$ and $|\psi_\downarrow(0)\rangle$. The Hamiltonian remains unchanged, and the states undergo a time evolution for around 300 D^{-1}.

In Fig. 3, we show the time dependence of two quantities in the case of σ^z measurement. First, for both states, we compute the time-dependent expectation value of the chirality Eq. (2) normalized by the ground-state chirality $Q_{GS} = \langle\psi_{GS}|\hat{Q}|\psi_{GS}\rangle$. Second, we analyze how much the quantum states change in time by computing the overlap $q_\gamma(t)$ between the state at time t with the state right after the projection:

$$q_\gamma(t) = |\langle\psi_\gamma(0)\,|\,\psi_\gamma(t)\rangle|, \text{ where } \gamma \in \{\uparrow, \downarrow\}. \tag{7}$$

Here, $|\psi_\gamma(0)\rangle$ should not be confused with $|\psi_{GS}\rangle$: the former denotes the state right after the projection, whereas the latter is the state before the projection.

For both $|\psi_\uparrow(t)\rangle$ and $|\psi_\downarrow(t)\rangle$, the chirality, which is shown with dark green dots, decreases slightly right after the measurement and then flattens, oscillating within a narrow range of values. The small fluctuations around the average value hint towards spin decoherence waves propagating through the system after the measurement [31,35–37].

The overlap $q_\gamma(t)$ exhibits highly nontrivial dynamics for both measurement outcomes. Once perturbed by the local projective measurement, the system can eventually strongly deviate from the original skyrmion ground state while approximately retaining its spin texture as encoded in Q. This is the first indication that quantum skyrmions indeed demonstrate stability in a certain sense. Although the external perturbation destroys the original state, throughout the evolution, the system remains within a manifold of states that, on the level of operator expectation values, can be regarded as the quantum skyrmion phase.

How does the dynamics change if the projection is now performed along an axis orthogonal to the external magnetic field? In that case, one might expect a stronger effect of quantum fluctuations on the structure of the skyrmion. In Appendix A, we show the time-dependent expectation value of the normalized chirality Q/Q_{GS} and the overlap $q_\gamma(t)$ for the case of σ^x measurement. The data is very similar to Fig. 3. For both $|\uparrow_x\rangle$ and $|\downarrow_x\rangle$ measurement outcomes, the chirality decreases after the projection and then stabilizes at a new level within a narrow range of values. Compared to the σ^z case, the decrease of Q/Q_{GS} is bigger and is not instantaneous anymore, but still very rapid. We again observe small fluctuations in Q that might be the result of spin decoherence wave propagation. The dynamics of the overlap $q_\gamma(t)$ indicates that the quantum state changes drastically, but the skyrmion does not break down completely.

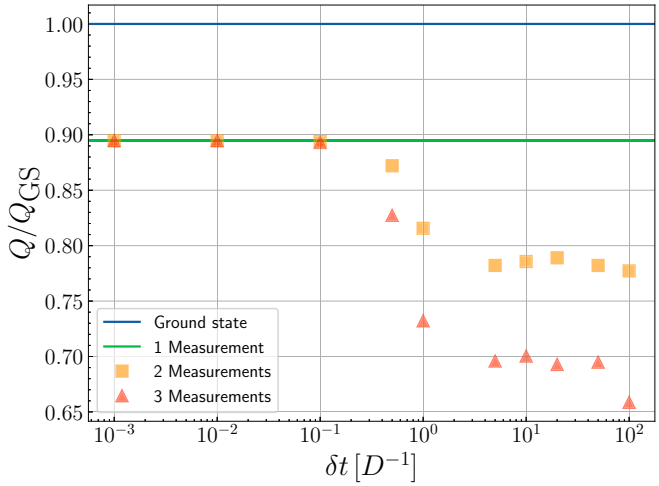

FIG. 4. Averaged normalized chirality for one and repetitive measurements as a function of time interval δt between measurements. Quantum Zeno effect stabilizes the quantum skyrmion when projective measurements are performed for time intervals below $\delta t \leqslant 0.1 D^{-1}$

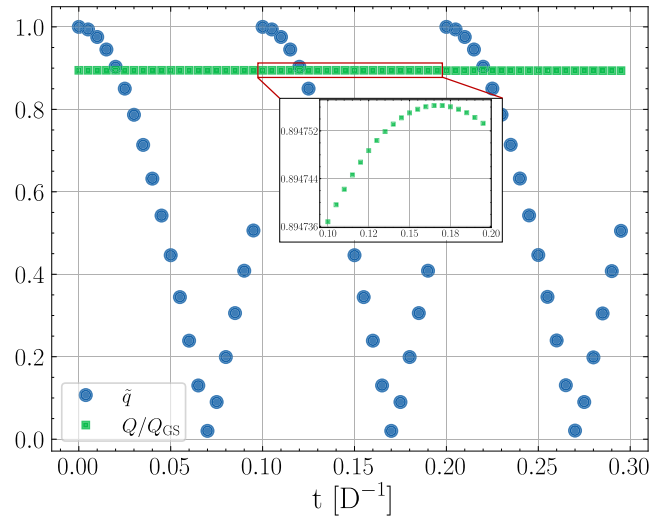

FIG. 5. Time evolution of the scalar chirality Q/Q_{GS} (green squares) and the overlap $\tilde{q}$ (blue circles) for three consecutive measurements. The measurements take place at $t = 0$, $t = 0.1\,D^{-1}$, and $t = 0.2\,D^{-1}$. The inset zooms in on the oscillations of the chirality.

IV. MULTIPLE MEASUREMENTS AND THE QUANTUM ZENO EFFECT

In the previous section, we have shown that the quantum skyrmion phase is robust with respect to a single local measurement. A natural question to ask is what happens to the quantum system when multiple measurements are performed sequentially: Will the measurements eventually destroy the quantum skyrmion or will they keep the system pinned to the manifold of states that can be regarded as the skyrmion phase? Here, we answer this question by systematically analyzing the effect of up to three consecutive measurements.

We start with the same ground state at $B = 0.5$ and perform up to three projective measurements of the z component of the central spin (additional data for the measurements of the x component are provided in Appendix A). The measurements are separated by a time interval δt during which the system undergoes the unitary evolution with Hamiltonian Eq. (1). We analyze how the resulting dynamics depends on the value of δt. As before, we start by discussing the scalar chirality Q.

Here, we compute Q immediately after the last measurement and average over all possible outcomes of the measurements

$$\begin{aligned} Q &= \mathrm{Tr}[\hat{Q}\rho], \\ \rho &= \sum_{\gamma_i \in \{\uparrow,\downarrow\}^{\otimes i}} p_{\gamma_i} |\psi_{\gamma_i}\rangle\langle\psi_{\gamma_i}|, \end{aligned} \tag{8}$$

where ρ is the von Neumann density matrix of rank 2^i, similar to Eq. (3), and $|\psi_{\gamma_i}\rangle$ is the state immediately after the sequence of measurements γ_i. The probabilities p_{γ_i} are given by the products of the individual outcome probabilities. For instance, $p_{\uparrow\downarrow\downarrow} = p_{1,\uparrow} \cdot p_{2,\downarrow} \cdot p_{3,\uparrow}$.

In Fig. 4, we show Q/Q_{GS} as a function of the time interval δt. For $\delta t > 0.1\,D^{-1}$, each subsequent measurement decreases the value of Q by around 10% of its original ground-state value, which implies that the quantum skyrmion is not robust upon multiple perturbations if they occur rarely enough. However, for shorter time intervals between the measurements, $\delta t \leqslant 0.1\,D^{-1}$, the subsequent measurements after the first one do not affect the value of Q.

Naively, one may suppose that the chirality expectation value does not really change in the regime of short inter-measurement intervals because the quantum state does not have time to significantly evolve between the measurements. To test whether this is the case or whether the roots of the robustness of Q are less trivial, consider the evolution of the wave function. For that, we define a weighted sum of overlaps as

$$\tilde{q}(t) = \begin{cases} \displaystyle\sum_{\gamma_1 \in \{\uparrow,\downarrow\}^{\otimes 1}} p_{\gamma_1} \cdot q_{\gamma_1}(t), & t \in [0, \delta t] \\ \displaystyle\sum_{\gamma_2 \in \{\uparrow,\downarrow\}^{\otimes 2}} p_{\gamma_2} \cdot q_{\gamma_2}(t - \delta t), & t \in [\delta t, 2\delta t] \\ \displaystyle\sum_{\gamma_3 \in \{\uparrow,\downarrow\}^{\otimes 3}} p_{\gamma_3} \cdot q_{\gamma_3}(t - 2\delta t), & t \in [2\delta t, 3\delta t] \\ \quad \ldots, \end{cases} \tag{9}$$

Here, $q_{\gamma_i}(t)$ is defined just as in Eq. (7), but with multiple consecutive projections. For $\delta t = 0.1\,D^{-1}$, the dynamics of this overlap is shown in Fig. 5 alongside the evolution of the scalar chirality. Note that after each measurement, the overlap is reset to 1 because we compute it with respect to not the original ground state but the state right after the corresponding projective measurement. It can be seen that the weighted overlap quickly deviates from 1, and the time-evolved states can essentially become orthogonal to the states of the system right after the measurement. After the first measurement, the relative change of Q is negligibly small, around 10^{-5}. In other words, the chirality is affected by neither measurements nor the interim unitary evolution. We suggest that this can be interpreted as a certain type of the QZE.

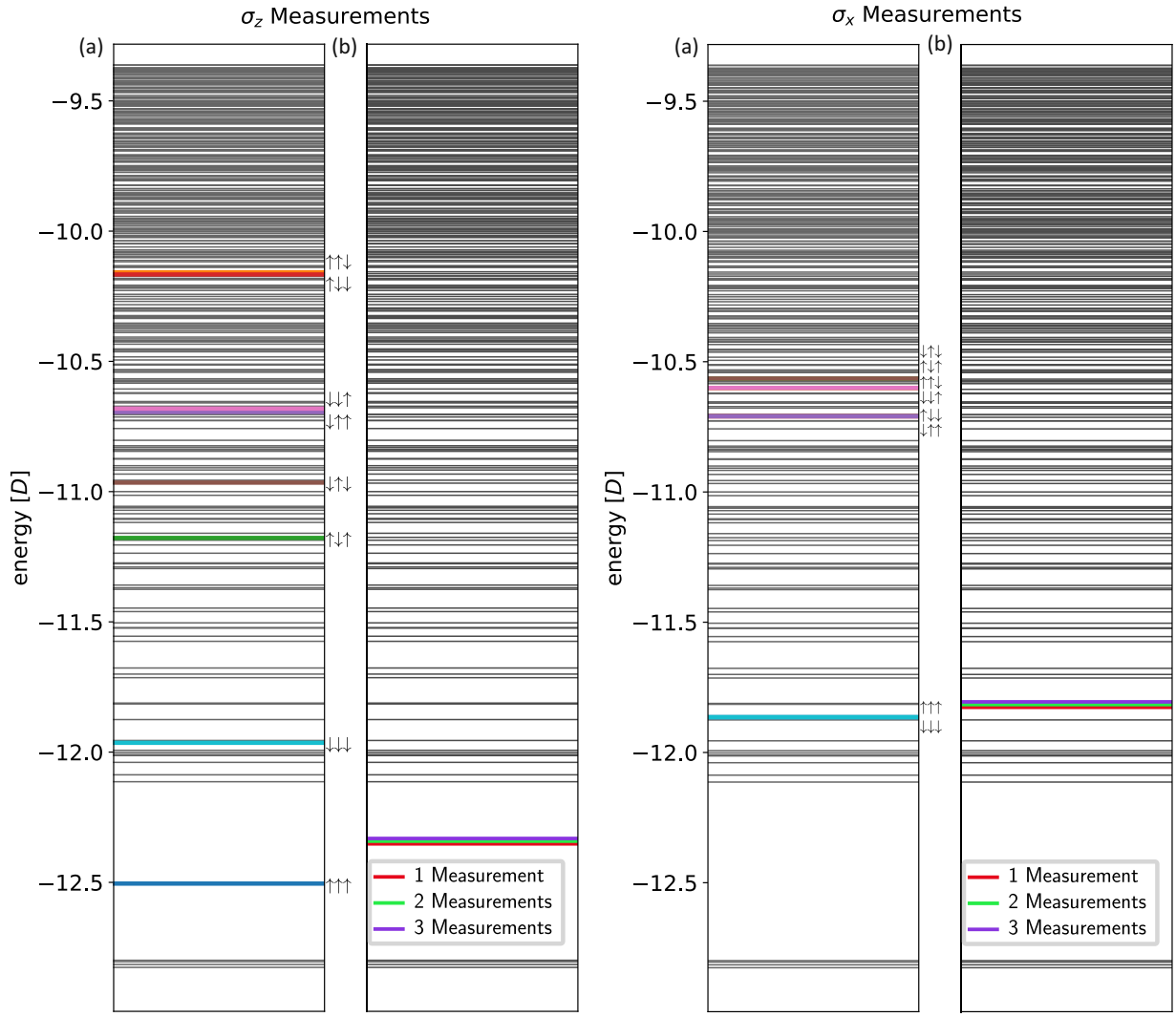

FIG. 6. The lowest part of the energy spectrum of the system. Energy levels are indicated with thin black lines. (a) Energies of different outcomes of projective measurements. (b) Energy of the system (i.e., weighted average the possible outcomes) for one, two, and three consecutive measurements of σ^z and σ^x.

In its simplest form, QZE means that a quantum system with a discrete spectrum that is monitored continuously (or, in practical terms, frequently enough) with von Neumann projective measurements cannot undergo a transition to another state even when its initial state is not stable [20]. Here, it is not quite the case since, after each measurement, the system rapidly evolves away from the initial state and the subsequent measurements do not bring it back. However, a broader class of QZE-like phenomena allows the system to nontrivially evolve in such a way that its state remains within a Zeno subspace defined by the measurement [21,22], and the studied case appears to fall into this category. In what follows, we will examine the process of Zeno stabilization in more detail and argue that QZE can be used to amplify the robustness of quantum skyrmions.

A similar analysis can be done for a few sequential same-site measurements in the σ^x-basis. As before, we compute Q immediately after each of the measurements by averaging over all possible outcomes of the sequence of preceding measurements. We again find (see Appendix A) that if the time between measurements is small enough, i.e., $\delta t \leqslant 0.1\, D^{-1}$, the quantum skyrmion remains robust. The robustness of the chirality is nontrivial as the weighted sum of overlaps Eq. (9) indicates that the system evolves far away from its original state—even becoming orthogonal to it—while retaining its skyrmionic nature. This behavior mirrors the scenario of multiple measurements in the σ^z basis, but whether it can be interpreted as a manifestation of the QZE will be discussed later.

V. FURTHER MANIFESTATIONS OF THE QUANTUM ZENO EFFECT AND THE SKYRMION ROBUSTNESS

A. Low-energy excitation spectrum

For the QZE scenario to be relevant, the quantum system's dynamics should involve states belonging to a discrete part of the energy spectrum. Although, formally speaking, the spectrum of a 19-spin system is discrete, some parts of it might transform into continuous bands upon increasing the

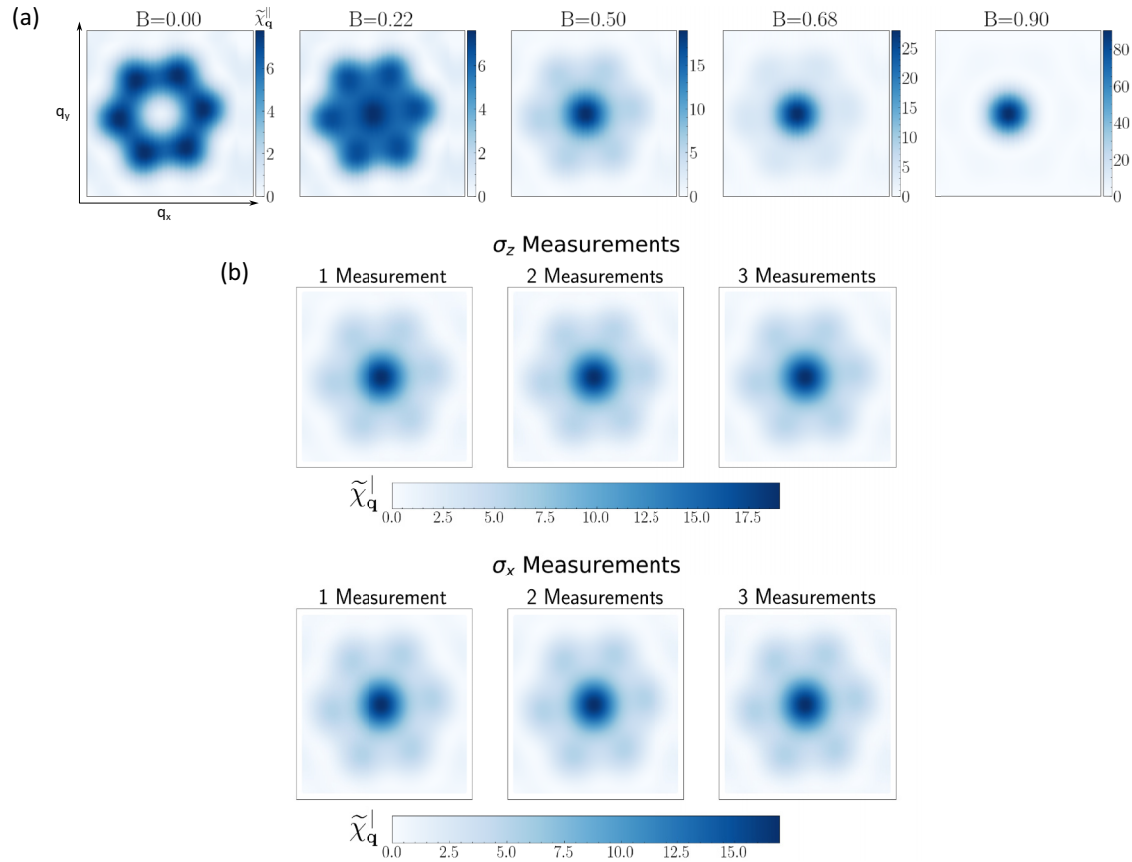

FIG. 7. The longitudinal spin structural factor of the system. (a) $X^{\parallel}_{\mathbf{q}}$ in the ground state for various values of the magnetic field B. (b) $\tilde{X}^{\parallel}_{\mathbf{q}}$ immediately after one, two, and three measurements of σ^z and σ^x. The value of the magnetic field is $B = 0.5$, and the time interval between the measurements is $\delta t = 0.1\, D^{-1}$.

system size to the thermodynamic limit. To see whether the measurement-driven dynamics of the quantum skyrmion occurs outside of such quasicontinuous parts of the spectrum, we study the spectrum of the system in more detail.

We use the lattice-symmetries [24] package to reconstruct the lowest-lying ∼1500 eigenstates. The energy spectrum is shown in Fig. 6. It has a large gap between a few nearly degenerate low-lying states and the quasicontinuum of higher excitations. Projective measurements drive the system from the ground state into a higher-energy state, and the energy after the measurements can fall into either the gap or the quasicontinuum, depending on the specific measurement outcomes, as shown in Figs. 6(a) and 6(c). For the σ^z measurements, the energy of the resulting state averaged over the von Neumann

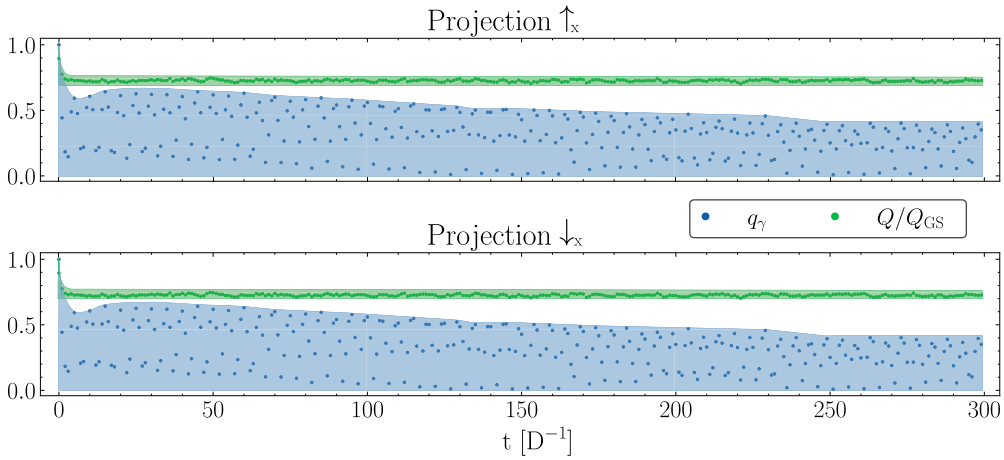

FIG. 8. Time evolution of the chirality Q (dark green dots) and overlap q_γ (blue dots) after one σ^x projective measurement. The top panel shows the projection onto $|\uparrow_x\rangle$ and the bottom panel onto $|\downarrow_x\rangle$. Lines and shades are a guide to eye.

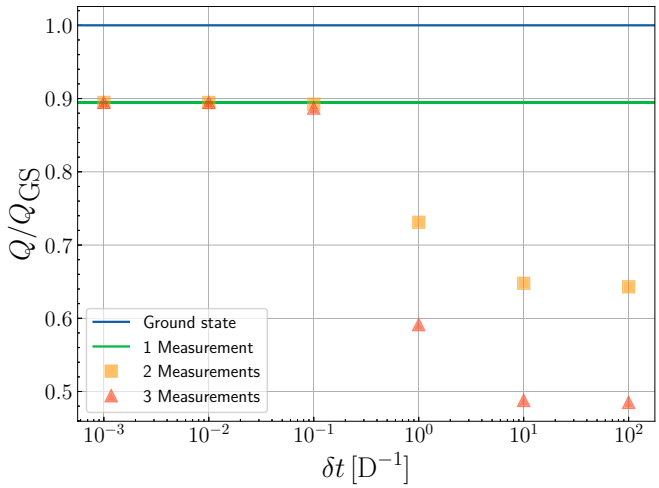

FIG. 9. Averaged normalized chirality for one and repetitive measurements of σ^x as a function of time interval δt between measurements. Quantum Zeno effect stabilizes the quantum skyrmion, when projective measurements are performed for time intervals below $\delta t < 0.1D^{-1}$. Note that the value of $Q/Q_{GS} \simeq 0.9$ immediately after the first measurement is higher than the value at which it eventually stabilizes in Fig. 8 due to the rapid continuous dynamics different from the observed in the σ^z case, and the QZE allows to stabilize chirality at values closer to its original value.

density matrix Eqs. (8) remains within the gap, Fig. 6(b). However, when the measurements are performed in the σ^x basis, both the individual outcomes and the overall mixed state (3) enter the part of the spectrum that can become a quasicontinuum in the thermodynamic limit. Hence, the QZE interpretation should be taken with care. However, there is still an indirect argument in favor of the QZE scenario. As we show in Appendix C, when sequential measurements are performed on different lattice sites, the scalar chirality decreases

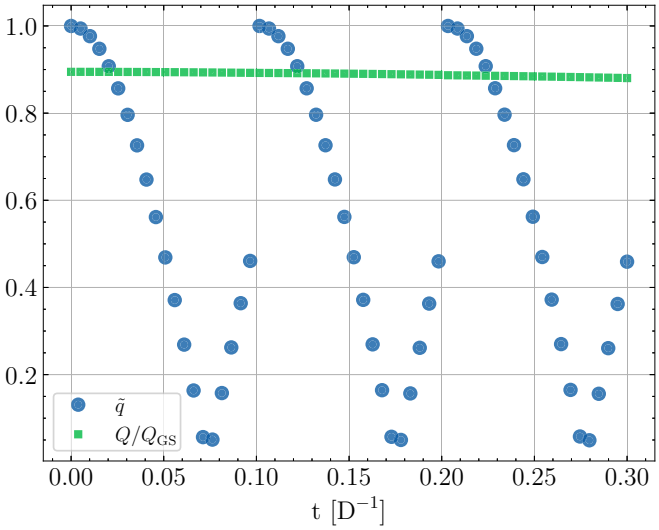

FIG. 10. Time evolution of the scalar chirality Q/Q_{GS} (green squares) and the overlap $\tilde{q}$ (blue circles) for three consecutive measurements of σ^x. The measurements take place at $t = 0, t = 0.1\,D^{-1}$, and $t = 0.2\,D^{-1}$.

with each measurement at approximately the same rate for both large and small δt. This implies that, in the multiple measurement setting, repeating the same measurement is critical for maintaining the robustness of the skyrmion, which is typical for the canonical QZE.

B. Longitudinal spin structural factor

Although the scalar chirality Q is the main characteristic feature of the quantum skyrmion phase, it cannot be probed experimentally due to the complexity of measuring three-point correlation functions. An alternative signature of a quantum skyrmion is the spin structural factor [38]

$$X^{\parallel}_{\mathbf{q}} = \langle S^z_{\mathbf{q}} S^z_{-\mathbf{q}} \rangle, \tag{10}$$

where $\mathbf{q}$ is scattering wave vector. $X^{\parallel}_{\mathbf{q}}$ can be measured in neutron scattering experiments [39], and in this section we analyze its robustness upon local projective measurements.

In Fig. 7(a), we show the intensity profile of the spin structural factor Eq. (10) calculated in the ground state of the Hamiltonian Eq. (1) for several different values of the magnetic field. Although in Ref. [10] it was argued that $X^{\parallel}_{\mathbf{q}}$ is a suboptimal probe of quantum skyrmion phase due to the lack of clear difference between the skyrmionic and helical states, here we see that the skyrmion has a recognizable pattern of Bragg peaks characterized by a strong zero-momentum peak and a halo of weaker peaks. If the pattern remains unchanged after a sequence of projective measurements, it would speak in favor of the operational robustness of quantum skyrmions.

The spin structural factor averaged over the measurement outcomes is

$$\tilde{X}^{\parallel}_{\mathbf{q}} = \sum_{\gamma_i} p_{\gamma_i} \langle \psi_{\gamma_i} | S^z_{\mathbf{q}} S^z_{-\mathbf{q}} | \psi_{\gamma_i} \rangle. \tag{11}$$

In Fig. 7(b), we show this quantity after one, two, and three projective measurements for both σ^z and σ^x. The profile of the structural factor remains nearly unchanged, with only a slight shift of intensity of the halo. Hence, we can safely claim that, on the level of observables (the scalar chirality and the spin structural factor), the quantum skyrmion phase is robust upon external local perturbations despite the absence of topological protection.

VI. CONCLUSIONS

We studied the robustness of a quantum skyrmion state with respect to local projective measurements using a 19-site triangular lattice as a model system. First, we analyzed the effect of the local projective measurements on the scalar chirality—a three-spin correlation function that can be considered a quantum analog of the skyrmionic topological charge [10,15]. The scalar chirality is not a topological charge and its robustness with respect to perturbations is not guaranteed. Nevertheless, we demonstrated that a local projective measurement has a relatively weak effect on the scalar chirality and reduces it by only around 10%.

Second, we analyzed the effect of up to three consecutive projective measurements and found that it depends on the time interval between the measurements. If the interval is small enough ($\lesssim 0.1\ D^{-1}$), an analog of the QZE arises and the

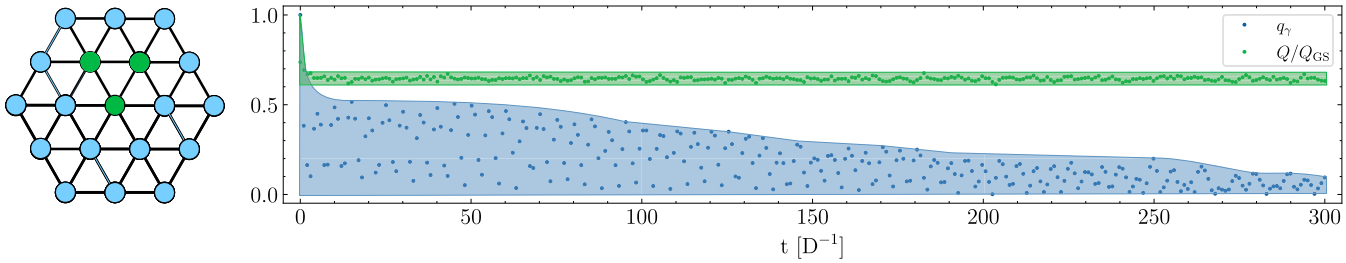

FIG. 11. Left: Single projective measurement in the σ^z basis performed on an elementary plaquette (shown with green dots). Right: Time evolution of the chirality Q (green curve) and overlap q_γ with the initial quantum state (blue dots).

skyrmion phase is stabilized by the measurements. Finally, in the quantum Zeno regime, we also demonstrate the robustness of the spin structural factor—the quantity that can serve as a signature of the skyrmion phase, but more easily accessible experimentally than the scalar chirality.

It is interesting to note that even outside of the QZE realm, for different types of single measurements—single-site σ^z and σ^x projections or simultaneous multiple-site projections (see Appendix B)—the resulting scalar chirality always stabilizes within a narrow window of values, even if the initial decrease is large, and the time evolution takes the underlying quantum state far away from the original wave function (up to complete orthogonality). This apparent discrepancy between the fragility of the quantum state and the stability of the corresponding observables would be interesting to explore in depth, and quantum skyrmions appear to be a good platform for that. Such operational stability also indicates that studying quantum skyrmions is a promising research direction with potential applications in reading and writing of information.

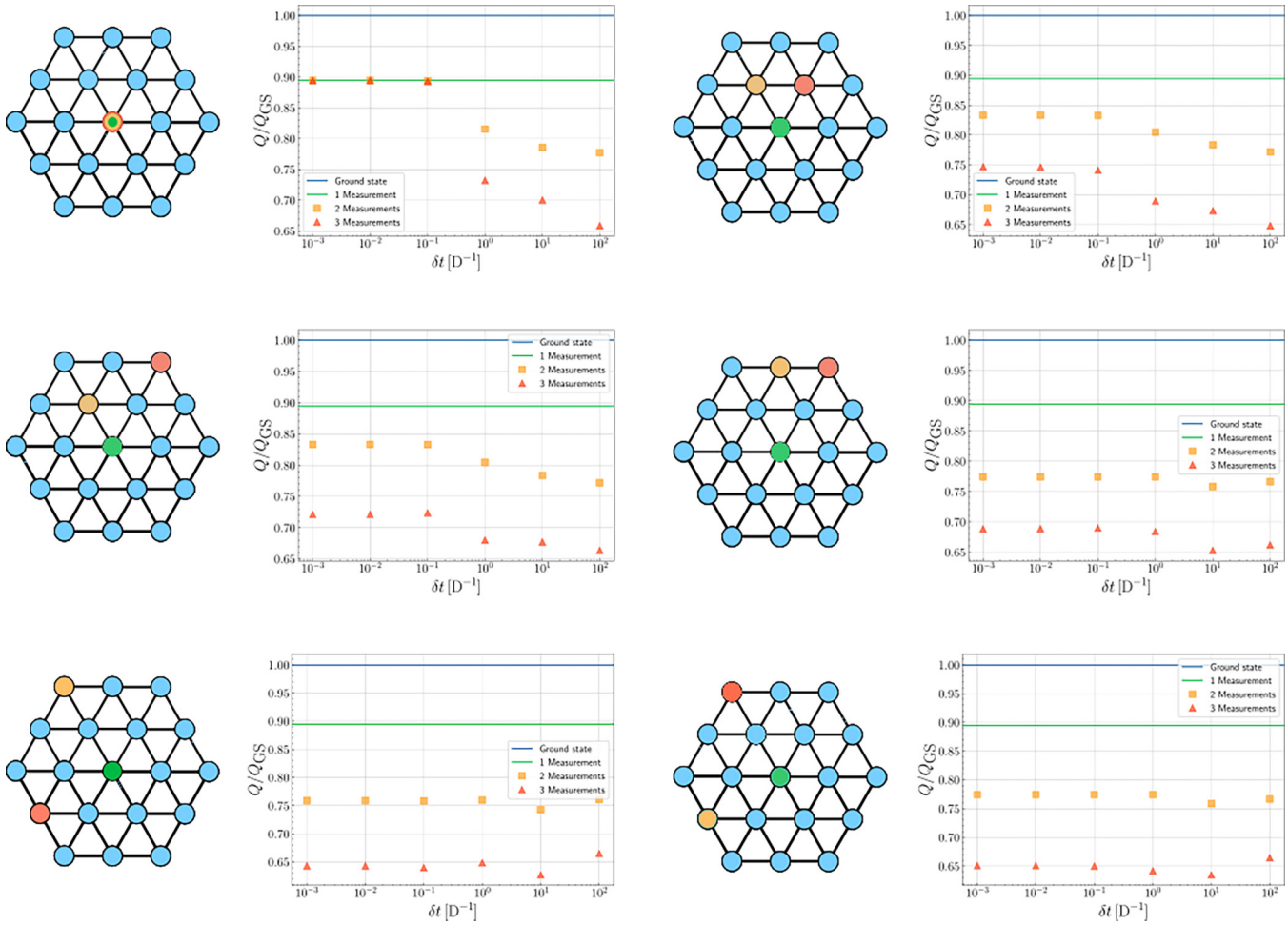

FIG. 12. Averaged normalized chirality after several projective measurements in the σ^z basis performed on different sites as a function of time interval δt between measurements. To the left of each plot, sites of measurements are shown in colors: the first measurement is on the green site, the second one—on the yellow, and the third one—on the red.

The data that support the findings of this paper are available from the corresponding author upon reasonable request.

ACKNOWLEDGMENTS

This work was supported by the European Research Council (ERC) under the European Union's Horizon 2020 research and innovation program, Grant Agreement No. 854843-FASTCORR.

APPENDIX A: MEASUREMENTS OF σ^x

In this Appendix, we show data for the case when σ^x is measured instead of σ^z. Figure 8 is the analog of Fig. 3 from the main text, Fig. 9—the analog of Fig. 4, and Fig. 10—the analog of Fig. 5.

APPENDIX B: SINGLE NONLOCAL MEASUREMENT

Single-site local measurements are just a specific type of projections that can be considered, and larger-scale or less symmetric perturbations can give a stronger shake to the quantum skyrmion, changing its properties in a more severe way. To probe the limits of the skyrmion stability, we first consider the case when a single projective measurement along the z axis is performed on several adjacent lattice sites—an elementary plaquette, Fig. 11. While this type of a more invasive perturbation naturally leads to a larger decrease in the value of chirality Q/Q_{GS}, it still stabilizes around a fixed value irrespective of how strongly the corresponding quantum state deviates from its initial conditions over the course of time evolution, as measured by the overlap $q_\gamma(t)$.

APPENDIX C: MEASUREMENTS ON DIFFERENT SITES

Another possible scenario is when several sequential local measurements are performed across the system at different locations. We restrict ourselves to considering σ^z measurements. The first measurement can be performed on any site, then the translational symmetry is broken and different configurations of the subsequent measurements can lead to different results. A few options are shown in Fig. 12. In contrast with repetitive measurements on the same site, here each subsequent measurement pushes the value of Q/Q_{GS} down, and the QZE-type dynamics does not emerge even for small intervals δt between the measurements. This is not unexpected, since the QZE assumes that measurements must be repetitive and not arbitrary.

[1] N. Nagaosa and Y. Tokura, Topological properties and dynamics of magnetic skyrmions, Nat. Nanotechnol. **8**, 899 (2013).

[2] R. Takashima, H. Ishizuka, and L. Balents, Quantum skyrmions in two-dimensional chiral magnets, Phys. Rev. B **94**, 134415 (2016).

[3] H. Ochoa and Y. Tserkovnyak, Quantum skyrmionics, Int. J. Mod. Phys. B **33**, 1930005 (2019).

[4] S. Mühlbauer, B. Binz, F. Jonietz, C. Pfleiderer, A. Rosch, A. Neubauer, R. Georgii, and P. Böni, Skyrmion lattice in a chiral magnet, Science **323**, 915 (2009).

[5] A. Neubauer, C. Pfleiderer, B. Binz, A. Rosch, R. Ritz, P. G. Niklowitz, and P. Böni, Topological Hall effect in the *a* phase of MnSi, Phys. Rev. Lett. **102**, 186602 (2009).

[6] N. Romming, C. Hanneken, M. Menzel, J. E. Bickel, B. Wolter, K. von Bergmann, A. Kubetzka, and R. Wiesendanger, Writing and deleting single magnetic skyrmions, Science **341**, 636 (2013).

[7] F. Jonietz, S. Mühlbauer, C. Pfleiderer, A. Neubauer, W. Münzer, A. Bauer, T. Adams, R. Georgii, P. Böni, R. A. Duine, K. Everschor, M. Garst, and A. Rosch, Spin transfer torques in MnSi at ultralow current densities, Science **330**, 1648 (2010).

[8] A. Fert, V. Cros, and J. Sampaio, Skyrmions on the track, Nat. Nanotechnol. **8**, 152 (2013).

[9] V. Lohani, C. Hickey, J. Masell, and A. Rosch, Quantum skyrmions in frustrated ferromagnets, Phys. Rev. X **9**, 041063 (2019).

[10] O. M. Sotnikov, V. V. Mazurenko, J. Colbois, F. Mila, M. I. Katsnelson, and E. A. Stepanov, Probing the topology of the quantum analog of a classical skyrmion, Phys. Rev. B **103**, L060404 (2021).

[11] A. Derras-Chouk, E. M. Chudnovsky, and D. A. Garanin, Quantum states of a skyrmion in a two-dimensional antiferromagnet, Phys. Rev. B **103**, 224423 (2021).

[12] J. P. Gauyacqm and N. Lorente, A model for individual quantal nano-skyrmions, J. Phys.: Condens. Matter **31**, 335001 (2019).

[13] P. Siegl, E. Y. Vedmedenko, M. Stier, M. Thorwart, and T. Posske, Controlled creation of quantum skyrmions, Phys. Rev. Res. **4**, 023111 (2022).

[14] K. Mæland and A. Sudbø, Quantum fluctuations in the order parameter of quantum skyrmion crystals, Phys. Rev. B **105**, 224416 (2022).

[15] V. V. Mazurenko, I. A. Iakovlev, O. M. Sotnikov, and M. I. Katsnelson, Estimating patterns of classical and quantum skyrmion states, J. Phys. Soc. Jpn. **92**, 081004 (2023).

[16] V. Vijayan, L. Chotorlishvili, A. Ernst, S. S. P. Parkin, M. I. Katsnelson, and S. K. Mishra, Topological dynamical quantum phase transition in a quantum skyrmion phase, Phys. Rev. B **107**, L100419 (2023).

[17] O. M. Sotnikov, E. A. Stepanov, M. I. Katsnelson, F. Mila, and V. V. Mazurenko, Emergence of classical magnetic order from Anderson towers: Quantum Darwinism in action, Phys. Rev. X **13**, 041027 (2023).

[18] N. D. Mermin, The topological theory of defects in ordered media, Rev. Mod. Phys. **51**, 591 (1979).

[19] J. von Neumann, *Mathematical Foundations of Quantum Mechanics—New Edition*, edited by N. A. Wheeler (Princeton University Press, Princeton, 2018).

[20] B. Misra and E. C. G. Sudarshan, The Zeno's paradox in quantum theory, J. Math. Phys. **18**, 756 (1977).

[21] P. Facchi and S. Pascazio, Quantum Zeno dynamics: Mathematical and physical aspects, J. Phys. A: Math. Theor. **41**, 493001 (2008).

[22] M. J. Aftab and A. Z. Chaudhry, Analyzing the quantum Zeno and anti-Zeno effects using optimal projective measurements, Sci. Rep. **7**, 11766 (2017).

[23] B. Berg and M. Lüscher, Definition and statistical distributions of a topological number in the lattice O(3) σ-model, Nucl. Phys. B **190**, 412 (1981).

[24] T. Westerhout, lattice-symmetries: A package for working with quantum many-body bases, J. Open Source Software **6**, 3537 (2021).

[25] S. Chowdhury, Comparing weak and projective measurements for quantum state tomography of a single-qubit system, arXiv:1711.03645.

[26] A. N. Jordan, B. Trauzettel, and G. Burkard, Weak-measurement theory of quantum-dot spin qubits, Phys. Rev. B **76**, 155324 (2007).

[27] S. Lloyd and J.-J. E. Slotine, Quantum feedback with weak measurements, Phys. Rev. A **62**, 012307 (2000).

[28] J. J. Sakurai, *Modern Quantum Mechanics (Revised Edition)* (Addison Wesley, Reading, MA, 1993).

[29] J. I. Cirac, D. Pérez-García, N. Schuch, and F. Verstraete, Matrix product states and projected entangled pair states: Concepts, symmetries, theorems, Rev. Mod. Phys. **93**, 045003 (2021).

[30] A. M. Gleason, Measures on the closed subspaces of a Hilbert space, J. Math. Mech. **6**, 885 (1957).

[31] H. C. Donker, H. De Raedt, and M. I. Katsnelson, Decoherence wave in magnetic systems and creation of Néel antiferromagnetic state by measurement, Phys. Rev. B **93**, 184426 (2016).

[32] H. Donker, H. De Raedt, and M. Katsnelson, Decoherence and pointer states in small antiferromagnets: A benchmark test, SciPost Phys. **2**, 010 (2017).

[33] M. Hernández, Chebyshev's approximation algorithms and applications, Comput. Math. Appl. **41**, 433 (2001).

[34] S. Yuan, H. De Raedt, and M. I. Katsnelson, Modeling electronic structure and transport properties of graphene with resonant scattering centers, Phys. Rev. B **82**, 115448 (2010).

[35] M. I. Katsnelson, V. V. Dobrovitski, and B. N. Harmon, Propagation of local decohering action in distributed quantum systems, Phys. Rev. A **62**, 022118 (2000).

[36] S. D. Hamieh and M. I. Katsnelson, Quantum entanglement dynamics and decoherence wave in spin chains at finite temperatures, Phys. Rev. A **72**, 032316 (2005).

[37] J. Chen, J. Hu, and H. Yu, Chiral emission of exchange spin waves by magnetic skyrmions, ACS Nano **15**, 4372 (2021).

[38] A. Haller, S. Groenendijk, A. Habibi, A. Michels, and T. L. Schmidt, Quantum skyrmion lattices in Heisenberg ferromagnets, Phys. Rev. Res. **4**, 043113 (2022).

[39] S. W. Lovesey, *Theory of Neutron Scattering from Condensed Matter: Volume 2. Polarization Effects and Magnetic Scattering* (Oxford University Press, United Kingdom, 1985).